Exchange-Induced Electron Transport in Heavily Phosphorus-Doped Si Nanowires

ARTICLE *in* NANO LETTERS · SEPTEMBER 2011

Impact Factor: 13.59 · DOI: 10.1021/nl202535d · Source: PubMed

NANO LETTERS

LETTER

pubs.acs.org/NanoLett

Exchange-Induced Electron Transport in Heavily Phosphorus-Doped Si Nanowires

Tae-Eon Park,[†,‡] Byoung-Chul Min,[‡] Ilsoo Kim,[†] Jee-Eun Yang,[§] Moon-Ho Jo,[§] Joonyeon Chang,[*,‡] and Heon-Jin Choi[*,†]

[†]Department of Materials Science and Engineering, Yonsei University, Seoul 120-749, Republic of Korea

[‡]Spin Device Research Center, Korea Institute of Science and Technology (KIST), Seoul 136-791, Republic of Korea

[§]Department of Materials Science and Engineering, Pohang University of Science and Technology (POSTECH), Pohang 790-784, Republic of Korea

ABSTRACT: Heavily phosphorus-doped silicon nanowires (Si NWs) show intriguing transport phenomena at low temperature. As we decrease the temperature, the resistivity of the Si NWs initially decreases, like metals, and starts to increase logarithmically below a resistivity minimum temperature (T_{min}), which is accompanied by (i) a zero-bias dip in the differential conductance and (ii) anisotropic negative magnetoresistance (MR), depending on the angle between the applied magnetic field and current flow. These results are associated with the impurity band conduction and electron scattering by the localized spins at phosphorus donor states. The analysis on the MR reveals that the localized spins are coupled antiferromagnetically at low temperature via the exchange interaction.

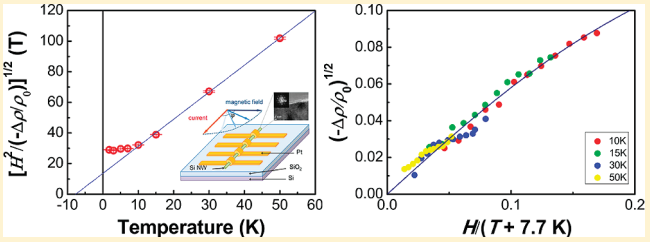

KEYWORDS: Silicon, nanowire, phosphorus, impurity band conduction, magnetoresistance, exchange interaction

Silicon nanowires (Si NWs) have been used as building blocks in the "bottom-up" approach to nanoelectronics because of their excellent electrical properties and hence have been studied for various applications, including field-effect transistors (FETs), chemical and biological sensors, and energy conversion devices.[1−5] In a different vein, spintronics, an emerging field of electronics based on the electron spin, is being intensively developed to overcome the limitation of conventional technology and to realize fast and energy-saving electronic devices.[6−8] To this end, various materials have been studied, including metals, oxides, semiconductors, and organic materials.[9−17] Group IV semiconductors are attractive materials for spintronics, owing to the weak spin−orbit coupling, large spin diffusion length, and compatibility with complementary metal-oxide semiconductor (CMOS) process.[18−20] The one-dimensional confinement, single crystalline structure, and long spin relaxation time of Si NWs provide an outstanding platform to study the spin injection/detection and transport in semiconductors. In particular, heavily doped Si NWs can provide an additional benefit for the spin injection into semiconductors, namely a reduced contact resistance at the ferromagnet/semiconductor interface.[19,20]

The transport and magnetoresistance (MR) of heavily doped bulk Si had been previously studied,[21−27] but the counterpart of Si NWs has remained relatively unexplored in detail. It is of interest whether the low-dimensional properties of Si NWs affect the transport and MR in heavily doped Si. As the impurity concentration becomes higher, the electrons which are localized at the donor sites start to interact with each other. This interactions of electrons in bulk Si:P system can be characterized by means of negative MR or electron spin resonance (ESR) measurements.[21−27] Sasaki *et al.* and Roth *et al.* reported that a negative MR could be observed in phosphorus-doped Si under certain impurity concentration condition below 4.2 K.[21,22] Maekawa *et al.* reported that the magnetic susceptibility obtained from the ESR spectra between 1.1 to 4.2 K shows an anomalous feature which has been considered to be related to the interaction of the localized moments between donor electrons.[24] These negative MR effects and ESR spectra in a phosphorus-doped Si system have been explained by Sonder et al. with the assumption that there exists antiferromagnetic exchange interaction between the donor electrons at low temperature.[28] Here we report on the interaction between the donor electrons and the exchange-induced transport properties of heavily phosphorus-doped Si NWs.

Heavily doped *n*-type Si NWs were synthesized by using vapor−liquid−solid (VLS) mechanism with silane (SiH_4) and a Au catalyst in a low-pressure chemical vapor deposition (CVD) system. Phosphorus doping was done by introducing phosphine (PH_3) into the input SiH_4 gas stream with a PH_3:SiH_4 gas flow ratio of 10^{-3}.[29,30] High-resolution transmission electron microscopy (HRTEM) image (Figure 1a) shows that the phosphorus-doped Si NW is single crystalline and structurally uniform. The fast Fourier transform (FFT) of the corresponding HRTEM image (the inset of Figure 1a) confirms that the growth orientation of the NW is in the ⟨110⟩ direction.

Figure 1b shows the scanning electron microscopy (SEM) image of a typical Si NW device geometry for electrical measurements

Received: July 25, 2011
Revised: September 6, 2011

dx.doi.org/10.1021/nl202535d | *Nano Lett.* XXXX, XXX, 000–000

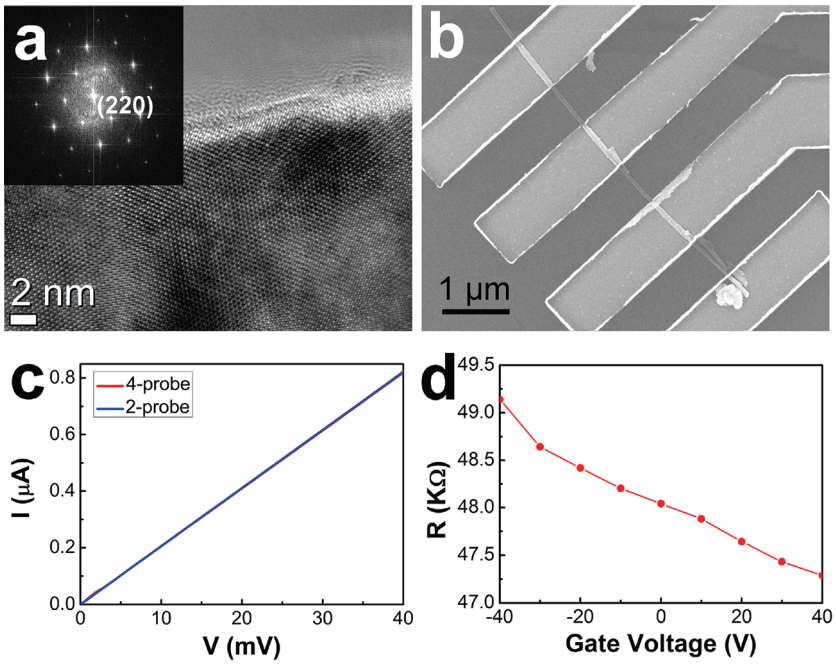

Figure 1. (a) HRTEM image of a heavily doped *n*-type Si NW. The inset is a FFT pattern of the corresponding HRTEM image, indicating that the growth direction of the NW is ⟨110⟩ direction normal to [−111]. (b) SEM image of a typical Si NW device geometry for electrical measurements consisting of four electrodes equally distributed on the NW with an intergap distance of 700 nm. (c) *I*−*V* characteristic of the Si NW measured by two- and four-probe geometries at room temperature. (d) Resistance of the Si NW as a function of the back gate voltage measured by the four-probe method.

consisting of four electrodes equally distributed on the NWs with an intergap distance of 700 nm. In order to fabricate the device geometry, the Si NWs were dispersed in an ethanol solution and spread onto p^+ Si substrate ($\rho \sim 0.01\ \Omega\cdot$cm) coated with a 500 nm-thick silicon oxide. This oxide layer can be used as a back gate dielectric layer. The electrical contacts were formed by electron beam lithography and lift-off process after removing the native oxide of the NWs by hydrofluoric acid. We have tested various metals for the electrical contacts, such as Ti (10 nm)/Au (70 nm), NiFe (80 nm), and Pt (80 nm). We find that all these metals can provide good ohmic contacts without any annealing, and the electrical properties of Si NWs do not depend on which metal is used for the electrical contact. Here we report the data obtained from the representative devices with Pt electrodes.

Figure 1c shows the *I*−*V* characteristics of a Si NW with a diameter of 50 nm measured by two- and four-probe geometries at room temperature. Two curves are almost linear in this voltage range and are exactly overlapped to each other, indicating that the contact resistances are almost negligible and that good ohmic contacts between the metal electrodes and the NW have been obtained. The resistivity of the Si NW is 13 m$\Omega\cdot$cm at room temperature with zero gate voltage, assuming that the Si NW is a perfect cylinder. The *I*−*V* characteristics depend on the back gate bias, as shown in Figure 1d. The resistance of the NW decreases with positively increasing gate voltage (Figure 1d), suggesting that electrons are the major carriers in this Si NW.

The weak dependence of resistivity on the gate voltage, low resistivity, low contact resistance, and linear *I*−*V* curves confirms that Si NWs are heavily doped *n*-type semiconductors. Unfortunately, it was challenging to determine the accurate doping concentration (n_d) and the mobility of the Si NW because it was very difficult to conduct the Hall measurement. Instead we have roughly estimated the n_d of the Si NW by comparing the measured resistivity of the Si NW at 300 K with bulk Si resistivity as a function of the phosphorus impurity concentration.[31] This gives a n_d of 3×10^{18} cm^{-3} but seems to be underestimated because the resistivity of the NW is usually enhanced due to the scattering at the NW boundary. It is well-known that the resistivity of thin films is always higher than the bulk resistivity and increases rapidly due to the size effect as the thickness decreases.[32] The estimated n_d of the Si NW can be regarded as a lower bound, and the real n_d can be considerably higher than 3×10^{18} cm^{-3}.

If the Mott criterion ($n^{1/3} > 0.25/\alpha_H$) is satisfied, then the carrier delocalization occurs, and material becomes conductive via the impurity band.[33−36] The critical carrier concentration can be estimated from the effective radius of the impurity atom, a_H, the dielectric constant of Si, and the conductivity effective mass of conduction electron.[31,35,36] It has been reported that, for $n_d > 3.74 \times 10^{18}$ cm^{-3}, the electrons exist in an impurity band with delocalization, and the metallic transition takes place in phosphorus-doped Si.[35] Taking into account the size effect, the n_d of the Si NW seems to be in the impurity conduction range. It has been also reported that, for $n_d > 2 \times 10^{19}$ cm^{-3}, the electrons on the Fermi level have the properties of those in the conduction band of pure Si, but for $n_d < 2 \times 10^{19}$ cm^{-3}, the electrons on the Fermi level do not have the same properties of the conduction band electrons.[27,33] The n_d of the Si NW is likely to be lower than this critical concentration.

We have investigated the temperature dependence of the resistivity of heavily phosphorus-doped Si NWs using a four-probe configuration from 1.8 to 300 K (Figure 2). As we decrease the temperature, the resistivity of Si NWs initially decreases and, unexpectedly, shows a resistivity minimum around 60 K (Figure 2a). Below the resistivity minimum temperature (T_{min}), we have observed that the resistivity increases logarithmically with

dx.doi.org/10.1021/nl202535d |*Nano Lett.* XXXX, XXX, 000–000

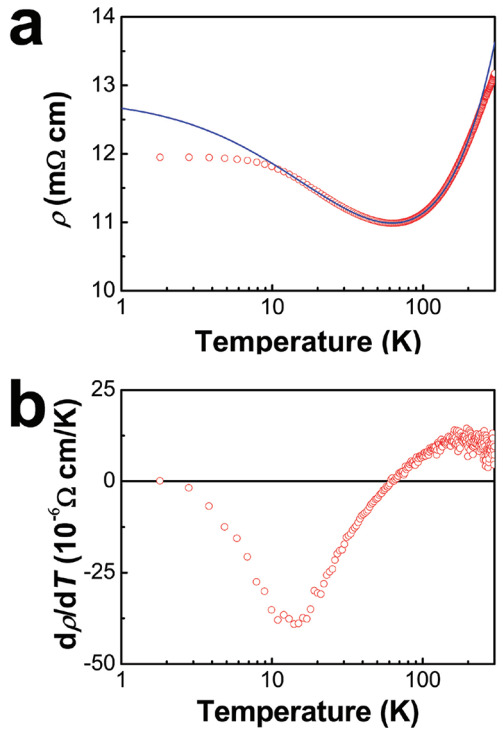

Figure 2. (a) Resistivity measured (red circle) as a function of temperature of a Si NW measured at I = 500 nA with four-probe geometry. The blue solid line is an empirical fitting curve. (b) Differential resistance ($d\rho/dT$) versus T curve, indicating the resistivity has a minimum at 60 K and an inflection point at 13 K.

decreasing temperature down to 10 K and approaches a saturation value below 10 K (Figure 2a). Usually the resistivity of low-doped Si at low temperature increases exponentially with an ionization energy of phosphorus donors of 45 meV due to freezing out of the carriers.[31] In contrast, the carrier concentration of Si in the impurity conduction regime remains almost constant at low temperature.[37] It is likely that the resistivity measurement reveals the temperature dependence of the mobility of carriers, which seems to be an innate signature of the impurity band conduction and the additional scattering process, which will be discussed below.

Figure 2b shows the differential resistivity ($d\rho/dT$) versus T curves, indicating the resistivity has a minimum at 60 K and an inflection point at 13 K. From the ρ versus T curve above 13 K, we have obtained the following empirical fit for the temperature dependence of the Si NW resistivity:

$$\rho(T) = a + bT - c\log_{10}(T + T_0)$$

where a, b, c, and T_0 are positive parameters.[38] In this fit, the electrical resistivity of Si NWs consists of the metallic part and the logarithmic part that becomes distinct at low temperature. The empirical fit is in good agreement with the measured $\rho-T$ curves (T > 13 K) of many Si NWs (not shown).

Figure 3a shows that $I-V$ curves measured with four-probe geometry at different temperatures. The $I-V$ characteristics present another peculiar feature in the temperature range below T_{min} when the differential conductance (dI/dV) is plotted as a function of the bias voltage (Figure 3b). At low temperature, these curves show a clear dip around zero bias, which is suppressed with increasing temperature and disappears near T_{min}. The

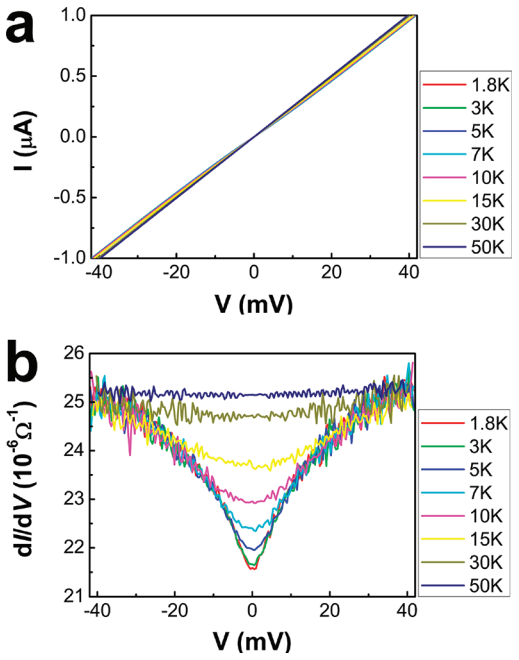

Figure 3. (a) Four-probe $I-V$ curves of a Si NW measured at different temperatures (1.8−50 K). (b) Differential conductance (dI/dV) of the Si NW as a function of bias voltage at different temperatures (1.8−50 K).

temperature range where the conductance dip is observed coincides with the range where the logarithmic increase of resistivity has been observed. This differential conductance dip suggests that an additional scattering process becomes dominant at a low bias.[39,40] It is believed that this zero bias anomaly is related to the scattering of conduction electrons with the localized spins existing in the impurity band of heavily doped n-type Si NWs.

The metallic behavior of the Si NWs (T > 60 K) can be well understood in terms of the high carrier concentration of the Si NWs ($n_d \geq 3 \times 10^{-18}$ cm^{-3}) and the impurity band conduction. The logarithmic temperature dependence that becomes dominant in the low-temperature range (13 < T < 60 K) is possibly associated with the existence of localized magnetic moments, which leads to the scattering of conduction electrons by the localized spins via an exchange interaction.[41,42] If this is the case, the phosphorus donor states are expected to be the only source of the localized spins, since no other magnetic impurities are included in the Si NWs. It has been reported that this kind of localized spin exists in the metallic impurity band of n-type InSb and Ge.[38,43] It is noteworthy that the T_{min}, where the logarithmic increase of resistivity becomes apparent, is quite high (T_{min} = ~60 K) in the Si NW in comparison with the cases with the heavily doped bulk InSb or other bulk semiconductors. This is possibly related to the size dependence of the resistivity contribution from the electron−phonon interaction in Si NWs.[44,45] Below 13 K, a significant divergence of $\rho-T$ curve from the empirical fit is observed as shown in Figure 2. In summary, the electrical resistivity of the NWs consists of the metallic resistivity originated from the phonon and impurity scattering and the spin-related resistivity associated with the scattering by localized spins, which gives rise to the logarithmic temperature dependence (13 < T < 60 K) and the saturation at low temperature (T < 13 K).

The most salient feature of the electron transport in the Si NW is the MR observed at low temperatures, as shown in Figure 4b.

dx.doi.org/10.1021/nl202535d |Nano Lett. XXXX, XXX, 000–000

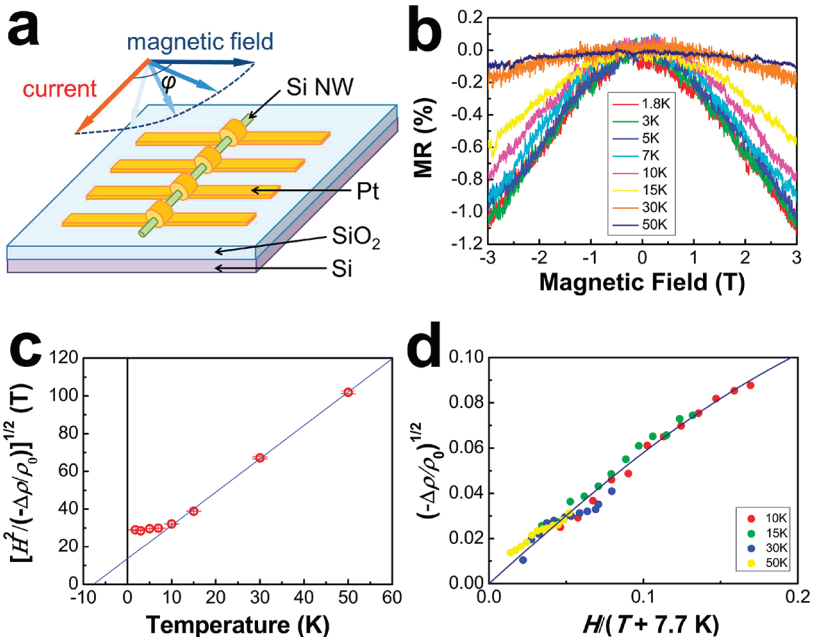

Figure 4. (a) A schematic representation of a Si NW device geometry. The device is subject to rotate in-plane. The φ indicates the angle of the applied magnetic field with respect to the Si NW axis (or current flow). (b) Temperature dependence of the MR of the Si NW measured at a current (I) of 500 nA with a magnetic field transverse to the Si NW axis (or current flow). (c) Temperature dependence of $[H^2/(-\Delta\rho/\rho_0)]^{1/2}$ (or $\alpha^{-1/2}\chi^{-1}$) in the Si NW. The blue solid line represents a function, $\alpha^{-1/2}\chi^{-1} = C/(T + 7.7\ \mathrm{K})$, where C is a positive constant. (d) Average magnetization of the localized spins $((-\Delta\rho/\rho_0)^{1/2})$ as function of $H/(T + 7.7\ \mathrm{K})$. The blue solid line is the Langevin function (classical Brillouin function).

As illustrated in Figure 4a, the magnetic field can be applied in arbitrary directions in the sample plane by rotating the sample with respect to the applied fields. We have measured the resistance of the Si NW at different temperatures (1.8−50 K) with applying external magnetic field. Figure 4b shows the MR of the Si NW with magnetic field transverse ($\varphi = 90°$) to the NW axis (or current flow) measured at $I = 500$ nA using four-probe geometry. The resistance decreases with the applied magnetic field (negative MR), and a nominal magnitude of MR defined by $\Delta\rho/\rho_0 = (\rho(H) - \rho(0))/\rho(0)$ is −1.1% at 1.8 K and −0.1% at 50 K at 3 T. The observed MR in Figure 4b is proportional to H^2, and the MR almost disappears at temperatures higher than T_{min}. This type of negative MR of the impurity conduction has been previously observed in a wide range of semiconductors, such as Si, Ge, SiC, InSb, and GaAs.[22,33,38,43,46,47] The Lorentz MR originated from the influence of the Lorentz force on the motion of electrons cannot explain this decrease of the resistance because, in the Lorentz MR effect, the resistance of Si NW should increase with the applied magnetic field. Moreover, given the small mobility of the electrons in the heavily phosphorus-doped Si NW, the Lorentz MR effect proportional to the square of the mobility seems to be significantly suppressed.[48]

Presumably, the observed negative MR can be related to the reduction of scatterings due to the alignment of the localized spins by the external magnetic field; the electrons scattering with randomly oriented localized spins contribute a high resistance, whereas the electron scattering with aligned spins results in a small resistance. Therefore, the negative MR in heavily doped Si NWs also reveals the exchange interaction between the conduction electrons and the localized spins, which will be discussed below.

The analysis on the temperature dependence of the negative MR provides a useful clue to understand the nature of the exchange interaction between the localized spins. Yosida has proposed that this negative MR is proportional to the square of the average magnetization of the localized spin system:[49]

$$-\Delta\rho/\rho_0 = \alpha M^2 = \alpha\chi^2 H^2$$

where M is the average magnetization of the localized spins, χ is the susceptibility of the localized spin system, H is the magnetic field, and α is a constant.[38,49] Following this proposition, the coefficient $\alpha\chi^2$ can be obtained from a parabolic fit of the MR versus H measurements (Figure 4b). Figure 4c shows a plot of the $[H^2/(-\Delta\rho/\rho_0)]^{1/2} = \alpha^{-1/2}\chi^{-1}$, which is inversely proportional to the susceptibility of the localized spin, as a function of the temperature (1.8−50 K). The parameter $\alpha^{-1/2}\chi^{-1}$ is proportional to $(T + T_0)$ above 10 K, following the Curie−Weiss law[38] and remains almost constant below 10 K. The positive T_0 implies that the exchange interaction among the localized spins is antiferromagnetic. It is also noteworthy that the T_0 is significantly large (~7.7 K), implying that the exchange interaction is quite stronger than those reported in bulk semiconductors.[27,38] The temperature range where $\alpha^{-1/2}\chi^{-1}$ is proportional to $(T + T_0)$ coincides with the range where the resistivity increases logarithmically, and the temperature range where $\alpha^{-1/2}\chi^{-1}$ remains constant corresponds to the range where the resistivity saturates to a constant (See Figure 2a). This result again shows that the resistivity of Si NW is closely related with the exchange interaction of the spin states in the impurity band.

The field dependence of the $(-\Delta\rho/\rho_0)^{1/2}$, which is proportional to the average magnetization of the localized spins, provides consistent features with the temperature dependence. The $(-\Delta\rho/\rho_0)^{1/2}$ values measured at different magnetic fields (0−3 T) and temperatures (10−50 K) are collapsed into a single curve when they are plotted as a function of $H/(T + 7.7\ \mathrm{K})$; otherwise they are scattered, for example, when they are plotted

dx.doi.org/10.1021/nl202535d |Nano Lett. XXXX, XXX, 000–000

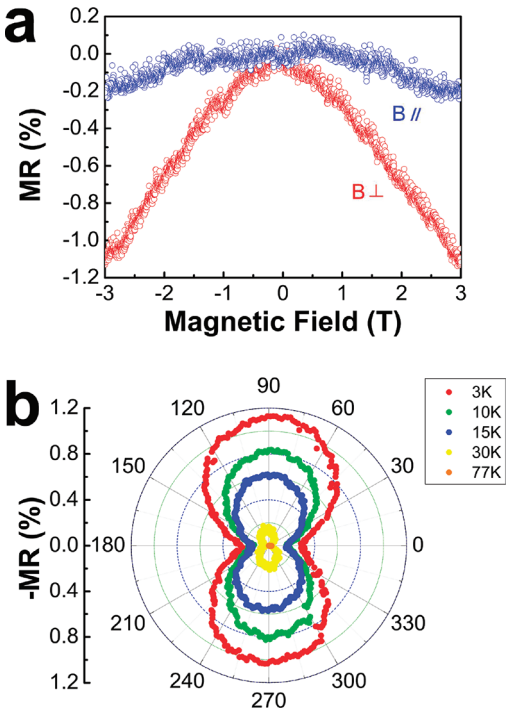

Figure 5. (a) Negative MR with a magnetic field applied transverse (red circle) and longitudinal (blue circle) to the Si NW growth direction ⟨110⟩ (or current flow) measured at I = 500 nA at 3 K. (b) Angular dependence of the MR measured at different temperatures with a current of 500 nA and a magnetic field of 3 T. The MR is plotted as a function of the in-plane angle between the magnetic field and the Si NW axis (or current flow), where the current flow direction is $\varphi = 0°$.

as a function of H/T. In addition, the curve which fits the $(-\Delta\rho/\rho_0)^{1/2}$ versus $H/(T + T_0)$ best has a form of the Langevin function (the classical Brillouin function),[38] as depicted in Figure 4d; the Langevin function is expressed as

$$\coth(\mu H/k(T + T_0)) - (k(T + T_0)/\mu H)$$

where μ is the net magnetic moment of the atom and k is Boltzmann's constant. This indicates that the localized spins can have arbitrary orientations with a local antiferromagnetic exchange interaction obeying the Curie−Weiss law. The temperature and field dependence of the negative MR unequivocally shows that the localized spins are coupled antiferromagnetically at low temperature via the exchange interaction in the impurity band.

Figure 5a shows a comparison of the negative MR with the magnetic field applied transverse ($\varphi = 90°$) and longitudinal ($\varphi = 0°$) to the growth direction ⟨110⟩ of the Si NW (or current flow) at 3 K. The MR shows a strong anisotropy; the transverse MR is −1.1%, whereas the longitudinal MR is only −0.2% at 3 T. In order to investigate the anisotropy of the MR in detail, we have measured the negative MR as a function of the angle between the magnetic field and the Si NW axis (or current flow) at different temperatures (Figure 5b). The MR shows a uniaxial anisotropy which persists up to T_{min}, and its magnitude is proportional to $\sin^2 \varphi$ plus a constant. We do not yet have a decisive explanation for the origin of the anisotropic MR (AMR). It is known that the AMR in 3d ferromagnetic metals is associated with the electronic structure of materials, spin−orbit interaction, and spin-dependent scattering between the conduction electrons and the localized spins.[50,51] It can be inferred that the AMR which we have observed in the heavily doped Si NWs can be understood based on a similar theoretical analysis. More study is required to clarify the origin of the anisotropy of the MR.

In conclusion, our experimental results show that the heavily doped *n*-type Si NWs present intriguing electrical and transport properties. The resistivity of the Si NW can be expressed as a combination of the typical metallic behavior and the logarithmic increase below T_{min}. The logarithmic increase of the resistivity is accompanied by: (i) the zero bias anomaly in the differential conductance measurement and (ii) the negative MR which can be understood in terms of the reduction of scatterings due to the alignment of the localized spins by the external magnetic field. The temperature and field dependence of the MR reveals that the localized spins are coupled antiferromagnetically at low temperature via the exchange interaction in the impurity band. In addition, this negative MR shows a strong angular dependence with respect to the angle between the applied magnetic field and the NW axis (or current flow). The concrete understanding of the transport phenomena of Si NW will provide a sound basis for studying the spin injection and detection in semiconductor NWs.

AUTHOR INFORMATION

Corresponding Authors

*E-mail: hjc@yonsei.ac.kr; presto@kist.re.kr.

ACKNOWLEDGMENT

This research was supported by a grant from the Nano R&D (2009-0082724), the National Research Laboratory Program (R0A-2007-000-20075-0), the Pioneer Research Program for Converging Technology (2009-008-1529) through the Korea Science and Engineering Foundation funded by the Ministry of Education, Science, and Technology, and the KIST institutional program.

REFERENCES

(1) Cui., Y.; Lieber, C. M. Functional Nanoscale Electronic Devices Assembled Using Silicon Nanowire Building Blocks. *Science* **2001**, *291*, 851–853.

(2) Cui., Y.; Zhong, Z.; Wang, D. I.; Wang, W. U.; Lieber, C. M. High Performance Silicon Nanowire Field Effect Transistors. *Nano Lett.* **2003**, *3*, 149–152.

(3) Cui., Y.; Wei, Q.; Park, H.; Lieber, C. M. Nanowire Nanosensors for Highly Sensitive and Selective Detection of Biological and Chemical Species. *Science* **2001**, *293*, 1289–1292.

(4) Tian, B.; Zheng, X.; Kempa, T. J.; Fang, Y.; Yu, N.; Yu, G.; Huang, J.; Lieber, C. M. Coaxial Silicon Nanowires as Solar Cells and Nanoelectronic Power Sources. *Nature* **2007**, *449*, 885–889.

(5) Hochbaum, A. I.; Chen, R.; Delgado, R. D.; Liang, W.; Garnett, E. C.; Najarian, M.; Majumdar, A.; Yang, P. Enhanced Thermoelectric Performance of Rough Silicon Nanowires. *Nature* **2007**, *451*, 163–167.

(6) Wolf, S. A.; Awchalom, D. D.; Buhrman, R. A.; Daughton, J. M.; von Molnar, S.; Roukes, M. L.; Chtchelkanova, A. Y.; Treger, D. M. Spinronics: A Spin-Based Electronics Vision for the Future. *Science* **2001**, *294*, 1488–1495.

(7) Zutic, I.; Fabian, J.; Sarma, S. D. Spintronics: Fundamentals and Applications. *Rev. Mod. Phys.* **2004**, *76*, 323–410.

(8) Chappert, C.; Fert, A.; van Dau, F. N. The Emergence of Spin Electroncis in Data Storage. *Nat. Mater.* **2007**, *6*, 813–823.

(9) Jedema, F. J.; Filip, A. T.; van Wees, B. J. Electrical Spin Injection and Accumulation at Room Temperature in an All-Metal Mesoscopic Spin Valve. *Nature* **2001**, *410*, 345–348.

dx.doi.org/10.1021/nl202535d |*Nano Lett.* XXXX, XXX, 000–000

(10) Parkin, S. S. P.; More, N.; Roche, K. P. Oscillations in Exchange Coupling and Magnetoresistance in Metallic Superlattice Strucutres: Co/Ru, Co/Cr, and Fe/Cr. *Phys. Rev. Lett.* **1990**, *64*, 2304–2307.
(11) Moodera, J. S.; Kinder, L. R.; Wong, T. M.; Meservey, R. Large Magnetoresistance at Room Temperature in Ferromagnetic Thin Film Tunnel Junctions. *Phys. Rev. Lett.* **1995**, *74*, 3273–3276.
(12) Delmo, M. P.; Yamamoto, S.; Kasai, S.; Ono, T.; Kobayashi, K. Large Positive Magnetoresistive Effect in Silicon Induced by the Space-Charge Effect. *Nature* **2009**, *457*, 1112–1115.
(13) Awschalom, D. D.; Flatte, M. E. Challenges for Semiconductor Spintronics. *Nature Phys.* **2007**, *3*, 153–159.
(14) Lou, X.; Adelmann, C.; Crooker, S. A.; Garlid, E. S.; Zhang, J.; Reddy, K. S. M.; Flexner, S. D.; Palmstrom, C. J.; Crowell, P. A. Electrical Detection of Spin Transport in Lateral Ferromagnet-Semiconductor Devices. *Nature Phys.* **2007**, *3*, 197–202.
(15) Koo, H. C.; Kwon, J. H.; Eom, J.; Chang, J.; Han, S. H.; Johnson, M. Control of Spin Precession in a Spin-Injected Field Effect Transistor. *Science* **2009**, *325*, 1515–1518.
(16) Schoonus, J. J. H. M; Bloom, F. L.; Wagemans, W.; Swagten, H. J. M.; Koopmans, B. Extremly Large Magnetoresistance in Boron-Doped Silicon. *Phys. Rev. Lett.* **2008**, *100*, 127202.
(17) Tombros, N.; Jozsa, C.; Popinciuc, M.; Jonkman, H. T.; van Wees, B. J. Electronic Spin Transport and Spin Precession in Single Graphene Layers at Room Temperature. *Nature* **2007**, *448*, 571–574.
(18) Appelbaum, I.; Huang, B.; Monsma, D. J. Electric Measurement and Control of Spin Transport in Silicon. *Nature* **2007**, *448*, 295–298.
(19) Min, B. C.; Motohashi, K.; Lodder, C.; Jansen, R. Tunable Spin-Tunnel Contacts to Silicon Using Low-Work-Function Ferromagnets. *Nat. Mater.* **2006**, *5*, 817–822.
(20) Dash, S. P.; Sharma, S.; Patel, R. S.; de Jong, M. P.; Jansen, R. Electrical Creation of Spin Polarization in Silicon at Room Temperature. *Nature* **2009**, *462*, 491–494.
(21) Sasaki, W.; Yamanouchi, C.; Hatoyama, G. M. *Proceedings International Conference on Semiconductor Physics, Prague*; Academic Press: Waltham, MA, 1960; p 159.
(22) Roth., H.; Straub, W. D.; Bernard, W. Empirical Characterization of Low-Temperature Magnetoresistance Effects in Heavily Doped Ge and Si. *Phys. Rev. Lett.* **1963**, *11*, 328–331.
(23) Yamanouchi, C.; Mizuguchi, K.; Sasaki, W. Electric Conduction in Phosphorus Doped Silicon at Low Temperatures. *J. Phys. Soc. Jpn.* **1967**, *22*, 859–864.
(24) Maekawa, S.; Kinoshita, N. Electron Spin Resonance in Phosphorus Doped Silicon at Low Temperatures. *J. Phys. Soc. Jpn.* **1965**, *20*, 1447–1457.
(25) Morigaki, K.; Maekawa, S. Electron Spin Resonance Studies of Interacting Donor Clusters in Phosphorus-Doped Silicon. *J. Phys. Soc. Jpn.* **1972**, *32*, 462–471.
(26) Ue, H.; Maekawa, S. Electron-Spin-Resonance Studies of Heavily Phosphorus-Doped Silicon. *Phys. Rev.* **1971**, *3*, 4232–4238.
(27) Quirt, J. D.; Marko, J. R. Absolute Spin Susceptibilities and Other ESR Parameters of Heavily Doped *n*-Type Silicon. II. A Unified Treatment. *Phys. Rev. B* **1973**, *7*, 3842–3858.
(28) Sonder, E.; Stevens, D. K. Magnetic Properties of *N*-Type Silicon. *Phys. Rev.* **1958**, *110*, 1027–1034.
(29) Wang, Y.; Lew, K. K.; Ho, T. T.; Pan, L.; Novak, S. W.; Dickey, E. C.; Redwing, J. M.; Mayer, T. S. Use of Phosphine as an n-Type Dopant Source for Vapor-Liquid-Solid Growth of Silicon Nanowires. *Nano Lett.* **2005**, *5*, 2139–2143.
(30) Ho, T. T.; Wang, Y.; Eichfeld, S.; Lew, K. K.; Liu, B.; Mohney, S. E.; Redwing, J. M.; Mayer, T. S. In Situ Axially Doped n-Channel Silicon Nanowire Field-Effect Transistors. *Nano Lett.* **2008**, *8*, 4359–4364.
(31) Sze, S. M. *Physics of Semiconductor Devices*; John Wilely & Sons: New York, 1969.
(32) Fuchs, K. The Conductivity of Thin Metallic Films according to the Electron Theory of Metals. *Proc. Cambridge Phil. Soc.* **1938**, *34*, 100–108.
(33) Alexander, M. N.; Holcomb, D. F. Semiconductor-to-Metal Transition in *n*-Type Group IV Semiconductors. *Rev. Mod. Phys.* **1968**, *4*, 815–829.
(34) Mott, N. F. On the Transition to Metallic Conduction in Semiconductors. *Can. J. Phys.* **1956**, *34*, 1356–1368.
(35) Kittel, C. *Introduction Solid State Physics*, 8th ed.; John Wilely & Sons: New York, 2005.
(36) Ramaneti, R.; Lodder, J. C.; Jansen, R. Kondo Effect and Impurity Band Conduction in Co:TiO_2 Magnetic Semiconductor. *Phys. Rev. B* **2007**, *76*, 195207.
(37) Pearson, G. L.; Bardeen, J. Electrical Properties of Pure Silicon and Silicon Alloy Containing Boron and Phosphorus. *Phys. Rev.* **1949**, *75*, 865–883.
(38) Katayama, Y.; Tanaka, S. Resistance Anomaly and Negative Magnetoresistance in *n*-Type InSb at Very Low Temperatures. *Phys. Rev.* **1967**, *153*, 873–882.
(39) Ralph, D. C.; Buhrman, R. A. Observation of Kondo Scattering without Magnetic Impurities: A Pint Contact Study of Two-Level Tunneling Systems in Metals. *Phys. Rev. Lett.* **1992**, *69*, 2118–2121.
(40) Calvo, M. R.; Fernanadez-Rossier, J.; Palacios, J. J.; Jacob, D.; Natelson, D.; Untiedt, C. The Kondo Effect in Ferromagnetic Atomic Contacts. *Nature* **2009**, *458*, 1150–1153.
(41) Kondo, J. Resistance Minimum in Dilute Magnetic Alloys. *Prog. Theor. Phys.* **1964**, *32*, 37–49.
(42) Toyozawa, Y. Theory of Localized Spins and Negative Magnetoresistance in the Metallic Impurity Conduction. *J. Phys. Soc. Jpn.* **1962**, *17*, 986–1004.
(43) Sasaki, W. Negative Magnetoresistance in the Metallic Impurity Conduction of n-Type Germanium. *J. Phys. Soc. Jpn.* **1965**, *20*, 825–833.
(44) Bid, A.; Bora, A.; Raychaudhuri, A. K. Temperature Dependence of the Resistance of Metallic Nanowire of Diameter >15 nm: Applicability of Bloch-Gruneisen Theorem. *Phys. Rev. B* **2006**, *74*, 035426.
(45) Mingo, N. Calculation of Si Nanowire Thermal Conductivity Using Complete Phonon Dispersion Relations. *Phys. Rev. B* **2003**, *68*, 113308.
(46) Sadasiv, G. Magnetoresistance in Germanium in the Impurity Conduction Range. *Phys. Rev.* **1962**, *128*, 1131–1135.
(47) Woods, J. F.; Chen, C. Y. Negative Magnetoresistance in Impurity Conduction. *Phys. Rev.* **1964**, *135*, A1462–A1466.
(48) Seeger, K. *Semiconductor Physics: An introduction*, 3rd ed.; Springer-Verlag: Berlin, Germany, 1985.
(49) Yosida, K. Anomalous Electrical Resistivity and Magnetoresistance Due to an *s-d* Interaction in Cu-Mn Alloys. *Phys. Rev.* **1957**, *107*, 396–403.
(50) Wegrowe, J. E.; Kelly, D.; Franck, A.; Gilbert, S. E.; Ansermet, J. Magnetoresistance of Ferromagnetic Nanowires. *Phys. Rev. Lett.* **1999**, *82*, 3681–3684.
(51) Smit, J. Magnetoresistance of Ferromagnetic Metals and Alloys at Low Temperatures. *Physica* **1951**, *17*, 612–627.

NOTE ADDED AFTER ASAP PUBLICATION

This article was published ASAP on September 26, 2011. Production errors were corrected in the equations on the third, fourth, and fifth page of the manuscript. The corrected version was posted on September 29, 2011.